Optics Letters

Flipping interferometry with doubled imaging area

Noa Rotman-Nativ, Nir A. Turko, and Natan T. Shaked*

Department of Biomedical Engineering, Faculty of Engineering, Tel Aviv University, Tel Aviv 69978, Israel
**Corresponding author: nshaked@tau.ac.il*

Received 10 September 2018; revised 10 October 2018; accepted 10 October 2018; posted 10 October 2018 (Doc. ID 344950); published 6 November 2018

We present a new external off-axis holographic module that doubles the acquired complex wavefront field of view, based on using both holographic flipping and multiplexing. In contrast to previous designs, this design does not require spatial filtering (no pinhole or lenses) to create the reference beam externally. In addition, the overlap area between the fields of view, as well as the off-axis angle between the sample and reference beams, can be fully controlled. As we demonstrate experimentally, this approach is useful for quantitative phase microscopy of extended stationary and dynamic samples, such as cancer cells during rapid flow and beating cardiomyocytes.

https://doi.org/10.1364/OL.43.005543

Imaging flow cytometry requires an extremely high frame rate to allow acceptable throughput when analyzing biological cells during flow. Cells *in vitro* are mostly transparent under regular light microscopy, and therefore cannot be imaged well without external stains or contrast agents, which might be harmful to the cells and are not allowed in certain medical procedures. Digital holography captures the quantitative phase profile, which takes into account the cell refractive index and physical thickness, using which one can obtain the cell quantitative topographic map with great contrast and without the need for external contrast agents. Furthermore, even if using contrast agents in flow cytometry, the fact that the phase profile is quantitative and accounts for the cell internal refractive indices gives rise to new parameters with medical relevance, which were not available in flow cytometry before, such as the dry mass of the cell. Off-axis holography [1–3] captures the complex wavefront of the sample within a single camera exposure, by inducing a small angle between the sample and reference beams creating the interference pattern of the hologram, which is highly relevant for quantitatively acquiring dynamic samples. This single-exposure mode is possible since the sample complex wavefront is fully separated from the other terms in the spatial frequency domain. This separation typically occurs across a single axis, which allows compressing more information on the other axes as well. This can be done by holographic multiplexing of several holograms with different interference fringe orientations into a single multiplexed hologram. Each wavefront from each hologram is fully separable from the other wavefronts due to being encoded with a different interference fringe orientation, and therefore all complex wavefronts can be fully reconstructed. Each of these complex wavefronts can contain additional data of the imaged sample, meaning that holographic multiplexing allows recoding more information with the same number of camera pixels. This is beneficial for highly dynamic samples, since more dynamic data can be recorded at once. In Ref. [4], we have proposed interferometry with doubled imaging area (IDIA), which optically projects onto the digital camera a multiplexed off-axis hologram with orthogonal fringe directions; each encodes a different field of view (FOV) of the sample, and both complex wavefronts can be fully reconstructed due to full separation in the spatial frequency domain. In this external holographic module, the reference beam is generated by spatial filtering of the sample beam using two lenses and a confocally positioned pinhole, and the two sample beams encoding the two FOVs are created by two orthogonally positioned two-mirror retroreflectors. In this module, the use of spatial filtering in the reference beam requires alignment of a pinhole, which impairs the system robustness. In Ref. [5], we proposed flipping interferometry (FI), which uses half of the optical beam as the reference beam for the other half and does not require pinhole alignment. This system is specifically suitable for acquiring biological cells during flow in a microfluidic channel, since the beam can be easily positioned on the border of the channel to allow a half-empty optical beam; however, this system is still inherently limited to acquiring a single FOV per exposure.

The current Letter presents flipping interferometry with doubled imaging area (F-IDIA), an external nearly common-path holographic module that combines both IDIA and FI, allowing the acquisition of doubled FOV by spatial multiplexing without using a pinhole alignment.

In Ref. [6], to implement FOV doubling, three mirrors were positioned between the tube lens and the camera, where the physical border between the mirrors does not allow a stitching area between the FOVs. More importantly, in this design, the off-axis angle, defining the off-axis spatial frequency of the fringes, and the area allocated for the reference beam are mutually dependent, in contrast to the design of the current Letter, which uses FOV flipping.

In Ref. [7], two-wavelength multiplexing of the same FOV was proposed using a module that contains two lenses, two

Corrected 7 November 2018

retro-reflectors, a mirror, and regular and polarizing beam splitters. In contrast to the current Letter, the two retro-reflectors are positioned in the Fourier domain of the lenses, which makes the system less suitable for FOV multiplexing; and the use of a polarizing beam splitter makes the system unsuitable for imaging polarizing samples.

Figure 1 shows a schematic illustration of the proposed system. A 5 mW, 632.8 nm, helium–neon laser illuminates an inverted microscope. The laser beam passes through the sample, is magnified by a 50×, 0.55-NA microscope objective, and passes through tube lens TL ($f = 200$ mm) to the F-IDIA module. In the F-IDIA module, beam splitter BS1 splits the beam into two beams. One beam is flipped and reflected back by retro-reflector RR, and is used as a reference beam. The second beam is split by beam splitter BS2 into two beams, and reflected by two slightly tilted mirrors M2 and M3 back to the camera. The mirrors create two orthogonal off-axis angles to avoid an overlap between the cross-correlation terms in the spatial frequency domain. A neutral density filter ND, located in front of the RR, equalizes between the light intensity that is reflected back from the RR and from each mirror, M2 and M3. Since we need to reduce the RR-reflected intensity by 50%, we choose a density filter of $-\log_{10}0.5 = 0.3$. The digital camera (Thorlabs, DCC1545M, 8 bit depth) is located at the image plane of the sample and records the multiplexed off-axis hologram in a single exposure.

As shown in the top-left inset in Fig. 1, the principle of operation is based on the assumption that the sample is placed across half of the optical beam, where the empty half is used as a reference. Thus, this method assumes that the beam projected onto the digital camera is much larger than the camera sensor size. Then, the RR flips the two halves of the beam. The titled mirrors M2 and M3 create orthogonal fringe patterns on the camera, with different FOVs from the imaged sample.

To experimentally demonstrate the principle of operation of the F-IDIA module, we first imaged the test target shown in Fig. 2(a), made by 200–400-nm-deep uneven laser engraving on glass (depth was verified by atomic force microscopy), using low-magnification (20× MO) bright-field microscopy, which enabled us recording the entire optical beam illuminating the sample, as indicated by the red circle in Fig. 2(a).

We then switched to high magnification (50× MO). In this case, only a small part of the sample could be imaged on the

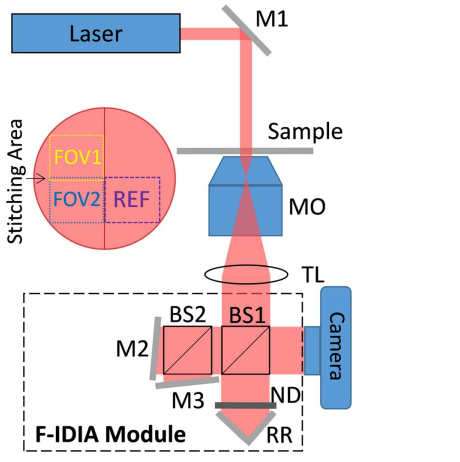

Fig. 1. Schematic illustration of the setup: an inverted microscope and the external F-IDIA module, for projecting a multiplexed off-axis image hologram on the camera, containing two FOVs, with the reference created by flipping. MO, microscope objective; TL, tube lens; M1, M2, M3, mirrors; BS1, BS2, beam splitters; RR, two-mirror retro-reflector; ND, neutral density filter.

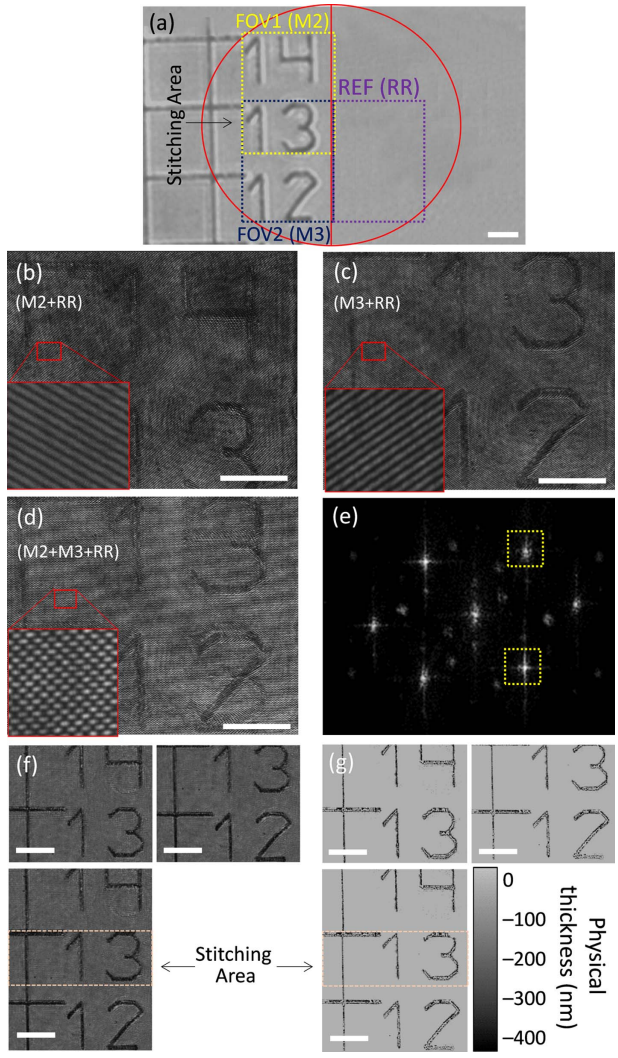

Fig. 2. Demonstration of the working principle of F-IDIA for imaging of a test target, made out of a glass surface with an uneven laser engraving. (a) Low-magnification bright-field microscopy of the test target. The red circle shows the optical FOV, and the dashed-line boxes indicate the digital FOVs 1 and 2 and the reference beam area, REF. (b) High-magnification imaging through the system shown in Fig. 1, when only M2 and RR are enabled, presenting a regular off-axis hologram. (c) High-magnification imaging through the system shown in Fig. 1, when only M3 and RR are enabled, presenting another regular off-axis hologram, with orthogonal fringe direction in comparison to (b). (d) High-magnification imaging through the system shown in Fig. 1, when all M2, M3, and RR, are enabled, presenting the multiplexed off-axis hologram. (e) Spatial frequency power spectra obtained by a 2D Fourier transform of the multiplexed hologram shown in (d). The chosen cross-correlation terms, each containing another FOV of the sample, are marked by yellow broken-line boxes. (f) The resulting reconstructed intensity images obtained for FOVs 1 and 2 (top) and the stitched one (bottom). (g) The coinciding physical thickness maps, obtained from the quantitative phase maps. White scale bars represent 10 μm.

camera, which is indicated by the yellow rectangle marked by FOV1 in Fig. 2(a). However, when using F-IDIA, both FOV1 and FOV2 [indicated by the blue rectangle in Fig. 2(a)] are acquired at once, where the area indicated by the purple rectangle in Fig. 2(a) is used as the reference beam of the multiplexed hologram. Figure 2(b) shows the regular off-axis hologram created by M2 and RR when mirror M3 is blocked, where only FOV1 is acquired. Figure 2(c) shows the regular off-axis hologram created by M3 and RR when mirror M2 is blocked, where only FOV2 is acquired. Finally, Fig. 2(d) shows the multiplexed off-axis hologram when all M2, M3, and RR are active, containing fringe patterns in orthogonal directions; each direction encodes a different FOV of the imaged sample. After acquiring this multiplexed hologram in a single exposure, we digitally applied a single 2D Fourier transform, resulting in the spatial frequency power spectrum shown in Fig. 2(e). This power spectrum contains two off-axis cross-correlation complex conjugate pairs, each encodes a different FOV of the sample, and a cross-term between the sample beams in between that does not overlap with any of them. We next digitally cropped one cross-correlation element from each pair, as indicated by the yellow dashed-line boxes, centered each of them, and applied an inverse Fourier transform to each of them separately, yielding the complex wavefronts of both recorded FOVs, the intensity profiles of which are shown at the top in Fig. 2(f), and the stitched one, with extended FOV, is shown at the bottom. The coinciding physical thickness profiles obtained from the quantitative phase maps (taking $n_{\text{glass}} = 1.51$) are shown in Fig. 2(g). The stitching area can be fully controlled, and can be aligned and set based on the visible spatial details of a test target, as done in this demonstration, which limits the stitching accuracy to the smallest imaged detail.

We next used F-IDIA for scan-free quantitative phase imaging of biological cells, which are wider than a single digital FOV in the chosen 50× magnification, and thus cannot be typically imaged by an off-axis interferometer in single exposure without camera or sample scanning. Figure 3 shows two examples of microscopic diatom shells, where the top images present the multiplexed off-axis holograms, each containing two FOVs of the sample. These holograms were used to reconstruct the coinciding double-FOV optical path delay (OPD) profiles shown at the bottom. The reconstruction process included the complex wavefront extraction, as explained for the former example presented in Fig. 2, followed by applying 2D phase unwrapping on the phase argument of the results, to avoid 2π ambiguities [8]. We then multiplied by the wavelength (632.8 nm) and divided by 2π, yielding the OPD profiles. In this case, a smaller stitching area was chosen, as indicated in Fig. 3 by the yellow dashed-line boxes.

Since the two off-axis holograms share the same dynamic range on the camera, we next measured the spatial standard deviation of the OPD profile of a single channel with the result of 3.64 nm, and of each of the OPD profiles when multiplexing, with the result of 6.43 nm on average, demonstrating that the signal-to-noise ratio (SNR) decreased due to sharing the camera dynamic range. Depending on the sample absorption and the application, this SNR decrease may require using a camera with higher dynamic range.

Next, to show the potential for imaging flow cytometry, we imaged WM-266–4 cells that were derived from a metastatic site of malignant melanoma, flowing between two

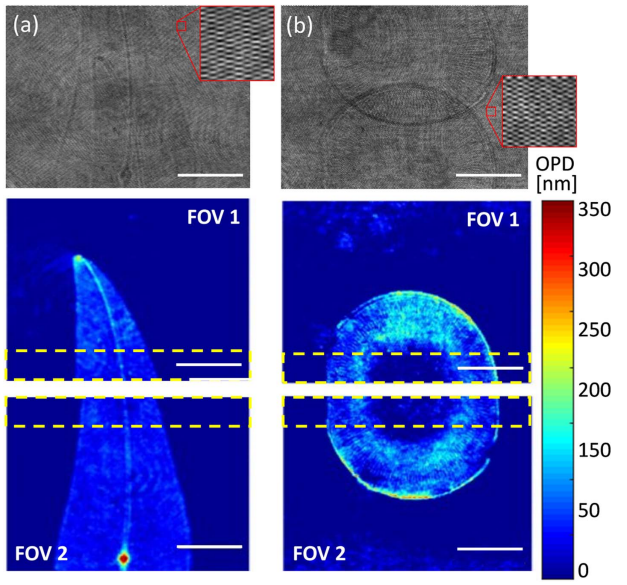

Fig. 3. Demonstration of F-IDIA for quantitative phase imaging of extended samples, which are larger than the camera imaging area. (a) and (b) present two different microscopic diatom shells that are spread on at least two FOVs and thus cannot be conventionally recorded in a single exposure without losing magnification or resolution. The top images present the multiplexed off-axis holograms, each containing the two FOVs at once. The bottom images present the reconstructed OPD maps of each diatom shell. The yellow broken-line boxes indicate the stitching area on each map. White scale bars represent 10 μm.

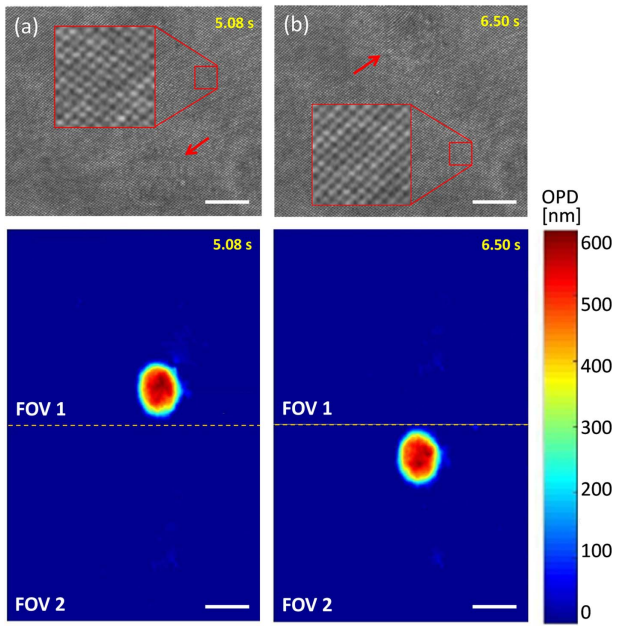

Fig. 4. Demonstration of F-IDIA for quantitative phase imaging of a single cancer cell flowing between two FOVs, while the camera does not need to track the cell: (a) at 5.08 s, the cell is in FOV1; (b) at 6.50 s, the cell is in FOV2. At each time point: top—the multiplexed off-axis hologram, containing the two FOVs; bottom—the stitched reconstructed OPD map. White scale bars represent 10 μm. See full dynamics in Visualization 1.

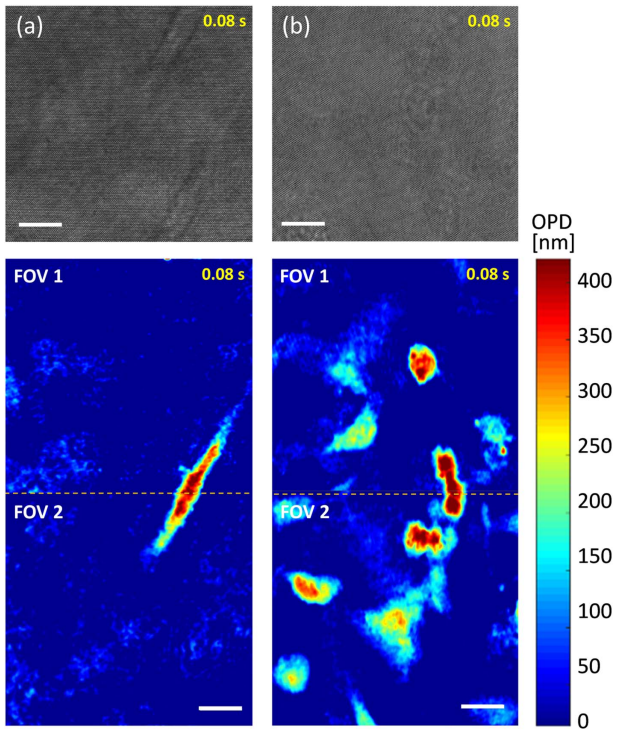

Fig. 5. Demonstration of F-IDIA for quantitative phase imaging of a beating cardiomyocyte monolayer, an extended dynamic sample that is larger than a single digital FOV. (a) and (b) show two different cardiomyocyte samples. The top image presents the multiplexed off-axis hologram, containing the two FOVs at once. The bottom image presents the stitched reconstructed OPD map. White scale bars represent 10 μm. See full dynamics in Visualization 2 and Visualization 3.

FOVs, without the need for moving the camera to track the cells during flow. The camera was positioned at the image plane on the edge of the channel, so that only half of the optical beam passed through the flowing area and the other half passed through the plane glass of the channel, allowing an interferometric reference beam area. Cells were grown in a flask. After cell density was 80%, they were trypsinized to disconnect from the flask, and then inserted into the 5 mL syringe. To induce cell flow, we used a micro-fluidic channel (Ibidi, 1 μ-Slide VI 0.1, 1 mm width, 17 mm length, 0.1 mm height). Figure 4(a) shows one frame of the dynamic cell flow, where the cell appears at the upper FOV, and Fig. 4(b) shows another frame of the dynamic cell flow, where the cell has already passed to the second FOV. In Fig. 4, the top images show the multiplexed holograms, and the bottom ones show the stitched double-FOV OPD profiles. The dynamic cell flow is shown in Visualization 1. Due to FOV doubling by holographic multiplexing, the camera was stationary during flow and did not track the cell.

Finally, we used the F-IDIA module for quantitative phase imaging of a beating cardiomyocyte monolayer. This sample is both wider than a single FOV and dynamic. Some researchers are interested in measuring the propagation of the beats across the cell monolayer. The multiplexed off-axis holograms of two different areas of the beating cardiomyocyte layer are shown in the top of Fig. 5, and the stitched double-FOV quantitative OPD profiles are shown in the bottom. The coinciding videos with the full dynamics are shown in Visualization 2 and Visualization 3.

To conclude, we have presented and experimentally demonstrated the portable F-IDIA module that can double the holographic FOV for complex wavefront acquisition with doubled imaging area using holographic multiplexing, and without the need for pinhole alignment due to using a retro-reflector to flip half of the FOV on top of the other one. We first demonstrated using the module for imaging digits engraved in glass, where the image of the sample was more extended than the sensor size under the magnification used. In spite of this, using F-IDIA, we acquired the entire magnified intensity and phase images by FOV stitching. Next, we demonstrated quantitative phase microscopy of diatom shells, which could not be imaged without scanning under the magnification used. Also in this case, we demonstrated that the entire diatom shell image can be acquired at once by extracting the two FOVs from the multiplexed hologram. Furthermore, we performed quantitative phase imaging of cancer cells during flow between two FOVs, without the need to shift the camera to track the cell during flow. This demonstration is highly relevant for imaging flow cytometry. Finally, we quantitatively imaged beating cardiomyocyte culture, which was larger than a single FOV. Here also, by using F-IDIA, this dynamic sample could be acquired at extended FOV. Although the off-axis angle (and hence the hologram spatial frequency) was optimal in all holograms acquired, we demonstrated various sizes of stitching areas in the module, which signifies the advantage of F-IDIA that the stitching area between the multiplexed FOVs can be changed independently of the off-axis angle. Therefore, F-IDIA does not suffer from ghost phase images (negative phase images that occur if the reference field is not empty), as long as half of the beam spot on the camera plane does not contain sample details. The proposed module is expected to be useful for imaging flow cytometry, where imaging throughput is critical.

Funding. German-Israeli cooperation grant in the field of Applied Nanotechnology, Israel Innovation Authority.

Acknowledgment. We thank Prof. Tal Dvir for providing us cardiomyocytes.

REFERENCES

1. H. Gabai and N. T. Shaked, Opt. Express **20**, 26906 (2012).
2. P. Girshovitz and N. T. Shaked, Biomed. Opt. Express **3**, 1757 (2012).
3. P. Girshovitz and N. T. Shaked, Opt. Express **21**, 5701 (2013).
4. P. Girshovitz and N. T. Shaked, Light Sci. Appl. **3**, e151 (2014).
5. D. Roitshtain, N. Turko, B. Javidi, and N. T. Shaked, Opt. Lett. **41**, 2354 (2016).
6. B. Tayebi, F. Sharif, M. Reza Jafarfard, and D. Y. Kim, Opt. Express **23**, 26825 (2015).
7. L. Liu, M. Shan, Z. Zhong, B. Liu, G. Luan, M. Diao, and Y. Zhang, Opt. Lett. **42**, 4331 (2017).
8. M. Arevallilo Herráez, D. R. Burton, M. J. Lalor, and M. A. Gdeisat, Appl. Opt. **41**, 7437 (2002).